Available online at www.sciencedirect.com
ScienceDirect
International Journal of Heat and Mass Transfer 51 (2008) 3514–3524
International Journal of HEAT and MASS TRANSFER
www.elsevier.com/locate/ijhmt

Large Eddy simulation of passive scalar in compressible mixing layers

C. Le Ribault

Laboratoire de Mécanique des Fluides et d'Acoustique, UMR CNRS 5509, Ecole Centrale de Lyon, Université Claude Bernard Lyon 1, INSA Lyon 36, avenue Guy de Collongue, 69134 Ecully, France

Received 4 April 2007; received in revised form 10 September 2007
Available online 29 January 2008

Abstract

Large Eddy simulations (LES) of compressible mixing layers are carried out to investigate scalar mixing. Convective Mach numbers of the simulations range from $M_c = 0.16$ to $M_c = 1.1$. In this study, the ability of two subgrid models (the dynamic Smagorinsky model and the dynamic mixed model) to predict scalar mixing in compressible shear layers is assessed. Comparisons of the results with experimental data show that the two subgrid closures are capable of capturing the principal effects of compressibility on scalar mixing, especially the decrease of scalar statistics and the changes in the shape of turbulent structures.

Keywords: Large Eddy simulation; Compressible flows; Passive scalar

1. Introduction

The role of compressibility in turbulent mixing layers remains an important issue in aeronautics, for example in the design of high-speed propulsion devices. The stabilizing effect of compressibility may reduce the efficiency of engines in mixing the fuel and the oxidizer.

A great number of experimental studies have shown a clear trend of reduced mixing layer growth rates with increasing Mach numbers [1–6]. The convective Mach number M_c, introduced by Bogdanoff, measures the intrinsic compressibility of a mixing layer. Assuming equal specific heats, the convective Mach number is equal to $M_c = \frac{U_1 - U_2}{c_1 + c_2}$ where U_1, c_1 denote the velocity and the speed of sound in the high-speed stream and U_2 and c_2 denote the corresponding quantities in the low-speed stream. Studies have shown that in addition to decreasing mixing layer growth rates, compressibility acts to suppress turbulence intensities and Reynolds stress [2,3]. Several experiments and numerical studies using both linear stability theory and direct simulations have shown that at low compressibility ($M_c < 0.6$), the structure is dominated by the two dimensional Kelvin Helmholz instability [1,4,7]. At higher levels of compressibility, the dominant instability waves are oblique resulting in three-dimensional structures [4,7]. The effect of convective Mach number on the evolution of instabilities and large-scale structures has also been investigated by Sandham and Reynolds [8].

The physics of scalar mixing in low Mach number turbulent shear layers is well understood. However the study of scalar mixing in compressible, high Mach number shear layers is more problematic since the experimental ability to resolve small scale mixing is limited. Experiments were conducted in a two-stream planar mixing layer at different convective Mach numbers by Clemens and Mungal [4] and in axisymmetric mixing layers by Clemens and Paul [9]. In two-species shear layers, scalar mixing is also inhibited in the presence of compressibility (see Clemens [4]) which reduces the magnitude of mixture fraction fluctuations. Increasing the Mach number is also found to change the mixture fraction probability density functions and the shape of turbulent structures.

Numerically, most of the simulations have been performed for temporal evolving mixing layers. Those mixing

E-mail address: catherine.le-ribault@ec-lyon.fr

0017-9310/$ - see front matter © 2007 Elsevier Ltd. All rights reserved.
doi:10.1016/j.ijheatmasstransfer.2007.10.030

layers develop in time and not in space, from specified initial conditions. The streamwise direction is homogeneous and periodic boundary conditions are applied in this direction. Then, no inflow/outflow boundary conditions are necessary in this approach. DNS of temporal evolving mixing layers at different convective Mach numbers have been performed by Pantano and Sarkar [10]. The principal compressibility effects such as the reduction of the spreading rate and the turbulence intensities are predicted. The mixing of fuel and oxidizer in temporal evolving annular mixing layers has been studied with direct numerical simulation by Freund et al. [11]. In their study, convective Mach numbers of the simulations range from $M_c = 0.1$ to $M_c = 1.8$. Scalar mixing was analyzed with probability density functions and visualisation of the scalar concentration.

Temporal evolving mixing layers display the main characteristic of turbulence. Qualitative comparisons with experimental results of the dominant mechanisms can be made. But, such an approximation is not physical, for example in the case of an interaction between a free shear flow and shock waves. Then, sometimes it is necessary to perform simulations of spatially evolving mixing layer. LES of a spatially evolving mixing layer at the convective Mach number of 0.62 has been carried out to investigate scalar mixing by Sankaran and Menon [12]. These studies have established that the linear Eddy model (LEM) was capable of predicting scalar mixing in compressible mixing layers. But the convective Mach number was not high enough to obtain important compressibility effects.

Previous studies, discussed in another paper, have established that LES is capable of predicting the compressibility effects on the growth rate and on the Reynolds stress [13]. Large Eddy simulation (LES) is now carried out to investigate passive scalar mixing in compressible mixing layers. In the study of Sankaran and Menon [12], the gradient diffusion closure was unable of capture the physics of scalar mixing. However, in the case of the plane jet, the dynamic Smagorinsky model and the dynamic mixed model was capable of predicting the scalar mixing (Le Ribault et al. [14,15]). Results of Na [16] also showed that the dynamic mixed model is capable of predicting scalar transport in channel with Schmidt number up to 10. The ability of two subgrid models, the dynamic Smagorinsky model and the dynamic mixed model to predict scalar mixing in compressible shear layers at convective Mach numbers up to 1.1 is assessed in this study.

This article documents and provides a discussion of results of LES for the passive scalar in compressible mixing layers. The governing equations, the subgrid models, the numerical method and the simulation parameters are first detailed. Principal results of the growth rate and the Reynolds stress are briefly described in paragraph 6. Development of mean scalar profiles and of scalar statistics are presented in paragraph 7. In the last paragraphs, probability density functions and instantaneous scalar fields are discussed.

2. Governing equations

The flow is governed by the Navier–Stokes equations in their compressible form, representing mass conservation, momentum conservation and energy conservation. The Navier–Stokes equations in the LES approach are filtered. The top-hat filter with a filter width Δ is used.

The filtered equations were previously described in Le Ribault [13,14]. The subgrid stress tensor $q_{ij} = \widetilde{u_i u_j} - \tilde{u}_i \tilde{u}_j$ is modeled, either by the dynamic Smagorinsky model, either by the dynamic mixed model. The dynamic Smagorinsky model is also used for the subgrid terms appearing in the pressure equation.

Since the simulations are performed for constant scalar diffusivity, the non-dimensionalized filtered equations for the passive scalar can be written as

$$\frac{\partial \overline{\rho}\tilde{\xi}}{\partial t} + \frac{\partial}{\partial x_k}\overline{\rho}\tilde{u}_k\tilde{\xi} = \frac{1}{ReSc}\frac{\partial}{\partial x_k}\left(\overline{\rho}\frac{\partial \tilde{\xi}}{\partial x_k}\right) - \frac{\partial \overline{\rho} q_k^{\xi}}{\partial x_k} \tag{1}$$

where q_k^{ξ} represents the passive scalar subgrid term:

$$q_k^{\xi} = \widetilde{u_k\xi} - \tilde{u}_k\tilde{\xi} \tag{2}$$

The subgrid models (dynamic Smagorinsky and dynamic mixed models), developed for the velocity field are also applied to the passive scalar equation. The Smagorinsky model [17], for the passive scalar can be written as

$$q_k^{\xi} = -\alpha_t \frac{\partial \tilde{\xi}}{\partial x_k} \quad \text{with} \quad \alpha_t = C_{d\xi}\Delta^2|\overline{S}| \quad \text{and} \quad |\overline{S}|^2 = 2\overline{S_{pq}S_{pq}} \tag{3}$$

and

$$S_{pq} = \frac{1}{2}\left(\frac{\partial u_i}{\partial x_j} + \frac{\partial u_j}{\partial x_i}\right) - \frac{1}{3}\frac{\partial u_l}{\partial x_l}\delta_{ij} \tag{4}$$

The coefficient $C_{d\xi}$ is dynamically computed [18] and depends on the local structure of the flow. The constant $C_{d\xi}$ is artificially set to zero during the few instances when it is still negative.

Similar to the mixed model [19] for the velocity, the mixed model for the passive scalar is also the sum of a Smagorinsky part and a scale-similarity part.

$$q_k^{\xi} = -C_d^{\xi}\Delta^2|\overline{S}|\frac{\partial \tilde{\xi}}{\partial x_k} + \overline{\overline{u_k}\overline{\xi}} - \overline{\overline{u_k}}\,\overline{\overline{\xi}} \tag{5}$$

The constant of the Smagorinsky part is dynamically computed. This model takes advantage of the correct dissipation produced by the dynamic eddy-viscosity part while the similarity part allows other effects such as the backscatter of energy from subgrid-scales to resolved scales.

3. Numerical method and inflow conditions

Since the numerical method has already been largely described by Le Ribault [14] and summarized in [15,13], only its principal characteristics are recalled here.

For the Navier–Stokes equations, spatial derivatives are computed using a non uniform fourth-order compact scheme of Lele [20]. In order to ensure long-time nonlinear stability, a fourth-order nonuniform compact filter is applied to the field at each iteration. The value of the filter is optimized to keep to influence of the filter as weak as possible is set equal to 0.4983 for the low compressible mixing layers. The value $\alpha = 0.5$ corresponds to no filtering. The key problem of the separation between modeling and numerical errors was detailed in Le Ribault et al. [14]. A fourth-order Runge–Kutta scheme is used for the time integration.

For the passive scalar equation, a flux-corrected-transport, FCT, scheme of Zalesak [21] is used. This scheme had been chosen in DNS to make sure scalar remained between 0 and 1 and the same scheme has been kept for the LES computations [22,15]. A predictor stage is performed with a 1st-order upwind scheme which produces a monotone solution. The predicted solution is then modified by a corrector stage using the difference between a 4th-order compact evaluation and the low-order scheme. This correction is nonlinearly limited to avoid spurious numerical oscillations.

Concerning the boundary conditions, on the outflow, the upper and lower sidewall boundaries, non reflecting conditions of Thompson [23], based on the characteristic equations are used. Moreover, to isolate the interior of the domain from the effects of the boundary conditions, a buffer zone based on the approach of Hu [24] is used on the non reflecting boundaries.

At the inflow, a hyperbolic tangent profile is used for mean velocity:

$$U = \frac{U_1 + U_2}{2} + \frac{U_1 - U_2}{2} \tanh\left(\frac{y}{2\theta}\right) \tag{6}$$

where θ is the momentum thickness of the shear layer.

The same hyperbolic tangent profile is used for the passive scalar:

$$\xi = \frac{\xi_1 + \xi_2}{2} + \frac{\xi_1 - \xi_2}{2} \tanh\left(\frac{y}{2\theta}\right) \tag{7}$$

with $\xi_1 = 1.0$ and $\xi_2 = 0.0$, respectively. The value of θ used for the passive scalar is the same as that used for the mean longitudinal velocity profile. For the velocity, a broadband forcing representative of isotropic turbulence is utilized at the inflow and a lateral shape is applied such that the fluctuation intensity peaks in the shear layers on either side of the jet. The noise level produced by turbulence injection is equal to $q/\Delta U = 5\%$ in the shear layer. The injected turbulence is divergence free. The inlet profiles for the mean longitudinal velocity, the streamwise fluctuation intensity RMS(u) and the mean scalar are presented on the Figs. 1–3.

4. Simulation parameters

The convective Mach number $M_c = \frac{U_1 - U_2}{c_1 + c_2}$ measures intrinsic compressibility of a mixing layer. Mixing layers

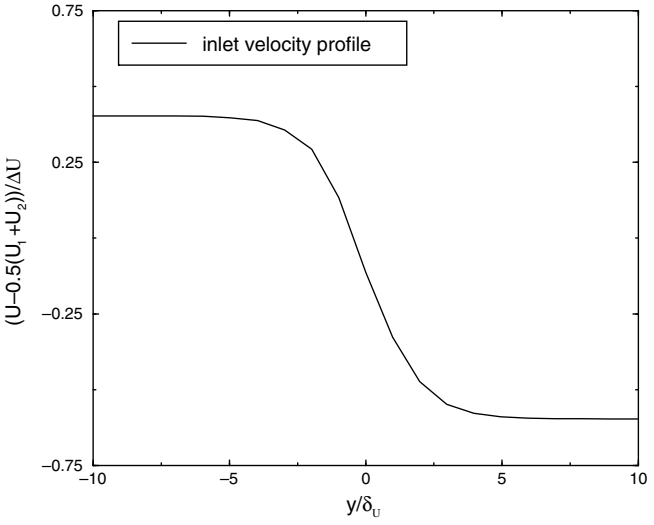

Fig. 1. Inlet mean streamwise velocity profile – $M_c = 0.16$.

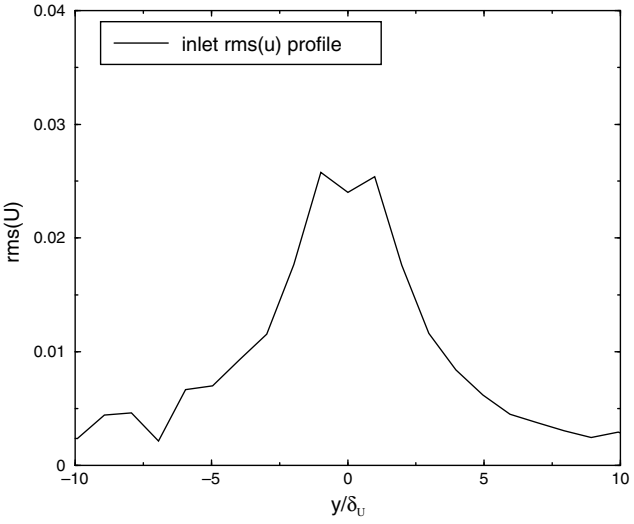

Fig. 2. Inlet RMS streamwise velocity profile – $M_c = 0.16$.

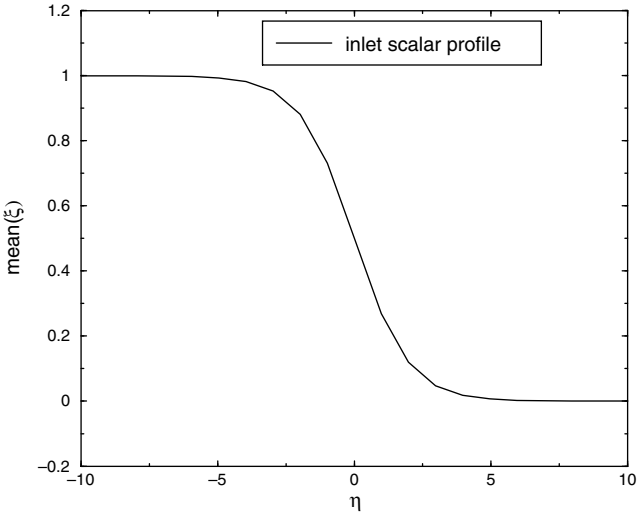

Fig. 3. Inlet mean scalar profile – $M_c = 0.16$.

at the convective Mach numbers of 0.16, 0.5 and 1.1 are simulated. At the convective Mach number of $M_c = 0.16$, compressibility effects are negligible. The convective Mach numbers of 0.5 has been chosen to correspond to the experiments of Elliot and Samimy [2]. where the compressibility effects are moderate. At the convective Mach number of 1.1, important compressibility effects are expected.

The Reynolds number, based on the inflow momentum thickness δ_{θ_0} and the velocity difference ΔU, is equal to $Re = \rho\delta_{\theta_0}\Delta U/\mu = 300$.

Preliminary computations have been performed on different grids to check the accuracy of the results. These computations particularly show the importance of taking a great number of nodes in the transversal direction z. To prove that present results are grid independent in the z direction, comparisons of evolution of momentum thickness on three different grids are presented on the Fig. 4. The size of the grid in the z direction remains the same but the number of grid points is respectively equal to 30, 50 and 60. The differences between the results are small, compared for example to differences providing from the convective Mach number.

Table 1 summarizes the dimensions of the computational domains and the number of grid points for the different cases. All the lengths have been non-dimensionalized by the inflow momentum thickness δ_{θ_0}. The resolution of scalar concentration is set by the Batchelor scale and is typically estimated with $\lambda_B \approx S_c^{-0.5}\delta_\xi Re_{\delta_\xi}^{-0.75}$ where δ_ξ denotes the layer thickness based on the passive scalar. Highly resolved measurements have suggested that the constant of proportionality is around 25.

The grid length increases with the convective Mach number because the length of the initial transient also increases with the convective Mach number. The grids have been kept as uniform as possible. In the y direction, the grid is very fine in the center of the mixing layer, then a slight stretching is used until the buffer zone.

Only one filter size $\Delta = 2h$, where h is the local grid spacing, is used.

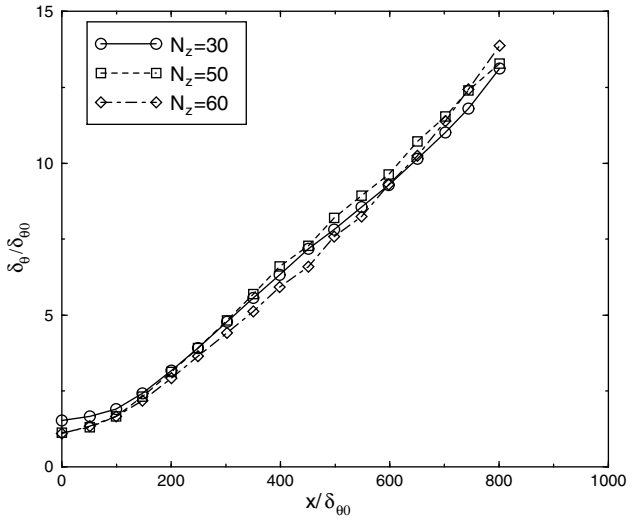

Fig. 4. Comparison of momentum thickness evolution obtained with the dynamic Smagorinsky model on three different grids – $M_c = 0.16$.

Table 1
Computational domains parameters

M_c	$L_x \times L_y \times L_z$	$N_x \times N_y \times N_z$	Resolution
0.16	$800 \times 144 \times 160$	$185 \times 119 \times 50$	$8\lambda_B \times 2\lambda_B \times 1.3\lambda_B$
0.5	$1000 \times 144 \times 80$	$227 \times 119 \times 50$	$8\lambda_B \times 2\lambda_B \times 2.5\lambda_B$
1.1	$2040 \times 820 \times 80$	$426 \times 179 \times 50$	$7\lambda_B \times 2\lambda_B \times 2.2\lambda_B$

5. Compressibility effects on the growth rate and on the Reynolds stress

In this paragraph, the main LES predictions for the decrease of the growth rate and the Reynolds stress components are summarized. All the results are detailed in [13].

An experimental curve, called "Langley curve" is obtained from the compilation of results coming from experiments with air–air shear layers. This curve gives the shear momentum thickness non dimensionalized by its incompressible counterpart as a function of the convective Mach number. Shear layer thickness growth rates predicted by the Langley curve have been plotted in the Fig. 5 along with the present LES results. The spreading rate of the mixing layers decreases with the convective Mach number in agreement with experimental results.

All the Reynolds stress components slightly decrease with the convective Mach number. Figs. 6 and 7 present the dependence of the peaks streamwise and transverse velocities on M_c. The results of the two turbulence models are compared with DNS results of Pantano and Sarkar [10] and with experimental results of Goebel and Dutton [5,6] and of Elliot and Samimy [2]. The difference between the experimental results are very important on those quantities. The LES results are closed to DNS results. For the

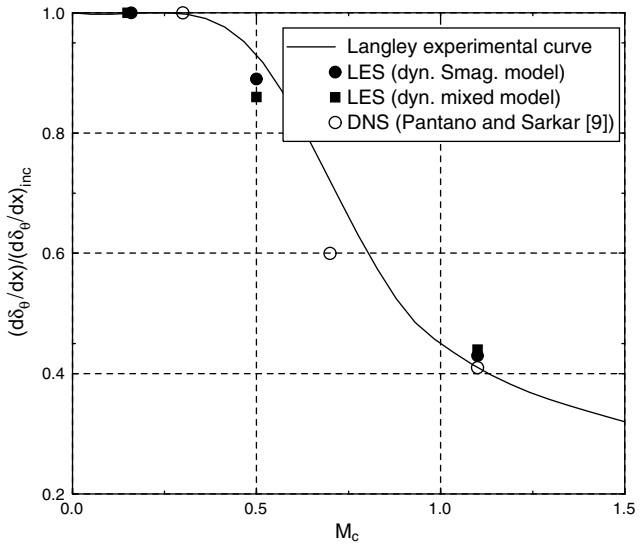

Fig. 5. Dependence of shear layer growth rate on M_c.

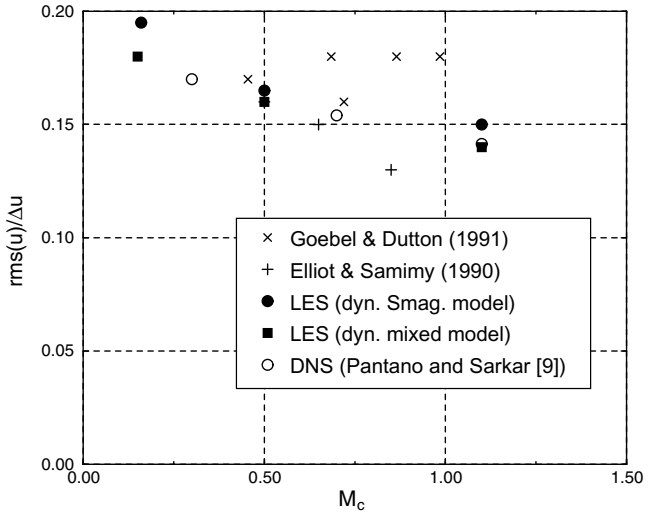

Fig. 6. Dependence of peak RMS streamwise velocity on M_c.

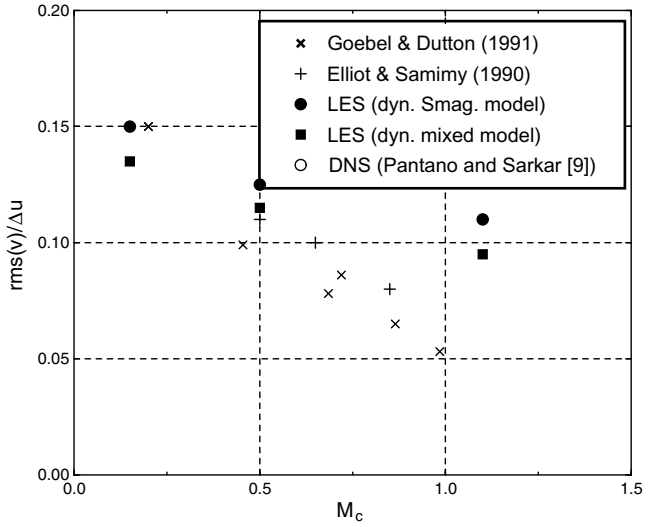

Fig. 7. Dependence of peak RMS vertical velocity on M_c.

streamwise intensity, the values predicted by the LES models are in the range of experimental data. The values of RMS(u) decrease even at the convective Mach number of 0.5. The decrease of RMS(v) is however less important than in experimental results. The dynamic mixed model predicts values slightly closer to experimental results than the dynamic Smagorinsky model but the difference between the two models prediction is weak.

The Figs. 8 and 9 present isovorticity contours obtained with the dynamic mixed model and the convective Mach numbers of 0.16 and 1.1 in the plane xy. Those figures confirm the increase of the transition zone with the convective Mach number. In the transition zone, the mixing layer thickness stay relatively constant, then the thickness increases linearly. For the $M_c = 0.16$ mixing layer, the roll-up and the pairing mechanism appears clearly. When the convective Mach number increases, the low Mach number organized structures are lost and the size of the structures decreases.

Concerning the overall prediction of the mean field and the Reynolds stress, both models are in agreement with experimental and DNS results.

6. Scalar mixing

This section provides a discussion of LES predictions of scalar mixing. Because scalar profiles are very similar at different Mach numbers, the full profiles are only provided for the lowest and highest Mach numbers.

After a transition zone, the mean passive scalar data collapse in self-similar like profiles. The profiles are plotted against a similarity variable, $\eta = (y - y_c)/\delta_\xi$. y_c is the transverse location with $(\xi - \xi_2)/(\xi_1 - \xi_2) = 0.5$ and δ_ξ is the thickness of the mixing layer defined as the distance between the transverse locations where $(\xi - \xi_2)/(\xi_1 - \xi_2)$ is 0.99 and 0.01. Fig. 10 shows the mean profiles obtained with the two subgrid models for the $M_c = 0.16$ case. Experimental results of Clemens and Mungal [4] obtained for $M_c = 0.28$ are plotted together. The profiles predicted by the two models are seen to be nearly identical. The mean profile shows a single inflection point, consistent with experimental observation of Clemens and Mungal [4]. Fig. 11 shows the mean profiles for the $M_c = 1.1$ case. There are no observable trends in the self-similar profiles shapes with increasing Mach number. The predictions of the two subgrid models collapse.

Root-mean squared concentration (RMS) fluctuations for the lowest and highest Mach numbers ($M_c = 0.16$ and $M_c = 1.1$) are plotted in Figs. 12 and 13. The self-similarity shape is predicted by the two models and the differences between the two predictions are small. The peaks are smaller at the convective Mach number of 1.1. The peak values predicted by the two subgrid models are plotted together with the experimental results of Clemens [4] in function

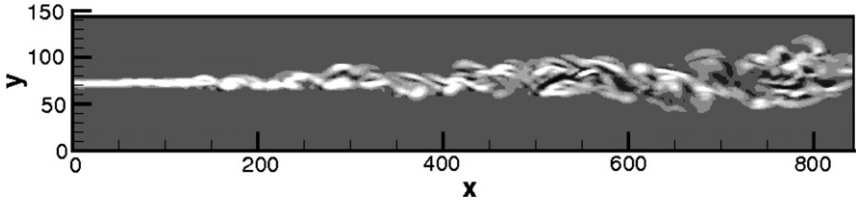

Fig. 8. Isovorticity in a $x - y$ plane – Dynamic mixed model – M_c=0.16.

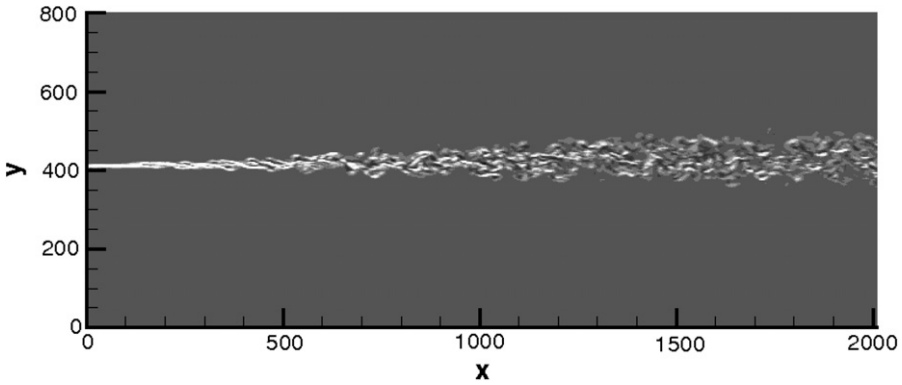

Fig. 9. Isovorticity in a $x-y$ plane – Dynamic mixed model – M_c=1.1.

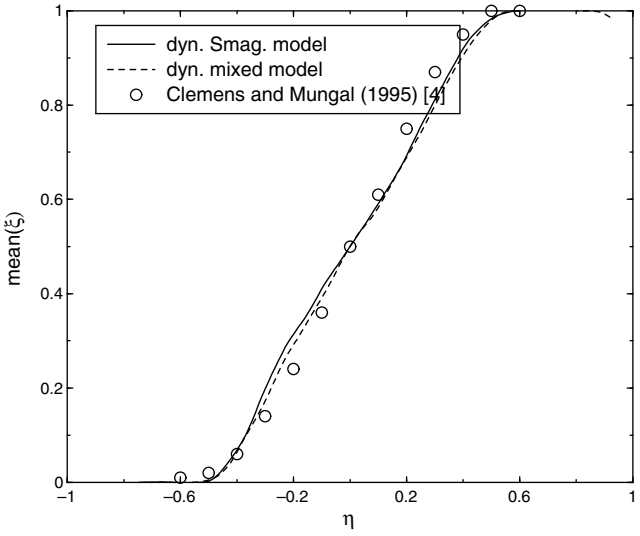

Fig. 10. Comparison of mean passive scalar obtained with the two subgrid models – $M_c = 0.16$.

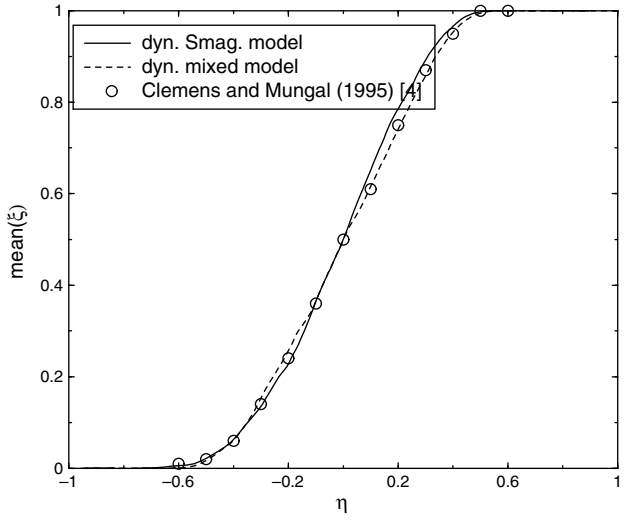

Fig. 11. Comparison of mean passive scalar obtained with the two subgrid models – $M_c = 1.1$.

of the convective Mach number (Fig. 14). The values are higher than those measured by Clemens and Mungal but under-resolution of those measurements may explain the difference. For a low convective Mach number, the peak fluctuations obtained by Clemens and Mungal [4] are about 17% whereas Konrad [25], Fiedler [26] and Batt [27] found fluctuations levels of 40%, 30% and 20%, respectively. Some experimentalists use the cold chemistry techniques to obtain quantitative mixing measurements that do not suffer from resolution errors (Island et al. [28], Clemens and Paul [9]). In the experiments of Clemens and Paul [9], the peaks RMS values decrease from 0.15 to 0.1 for convective Mach number varying from 0.35 to 1.3. But those results were obtained for axisymmetric mixing layers, so they are not presented on the Fig. 14. The Reynolds number also plays a role in the peak RMS value, the lower the Reynolds number, the higher the peak RMS is. Moreover the peak RMS values are higher in the pre-mixing transition and then decrease in the self-similarity region. The peaks of the RMS fluctuations predicted by the two LES models decrease with the convective Mach number. This is consistent with the experimental results of Clemens and Mungal where the fluctuations at $M_c = 0.28$ are about 15% greater than those at $M_c = 0.62$. In the DNS of Freund et al., the maximum values of RMS range from 0.31 at $M_c = 0.1$ to 0.22 for $M_c = 1.5$.

Profiles of the scalar fluxes for the $M_c = 0.1$ and $M_c = 1.1$ cases are plotted in Figs. 15 and 16. No experimental results are available on those quantities. The axial and transversal scalar fluxes both decrease with the convective Mach number. This is in contradiction with the results of Freund et al. [11] that show a decrease of the radial component $\widetilde{v\xi}$ while the peak of the axial component $\widetilde{u\xi}$ remains nearly constant between the lowest and highest Mach numbers. However the mixing layers of Freund et al. were annular mixing layers. In the case of plane mixing layers, all the Reynolds stress components decrease with the convective Mach number. In the case of the plane jet, the DNS of Pantano and Sarkar [10] and the LES of Le Ribault [15] show that the anisotropie tensor is strongly affected by M_c during the initial transient and then approaches asymptotic values that are weakly dependent on M_c. This may explain why scalar fluxes peaks also have an isotropic behavior.

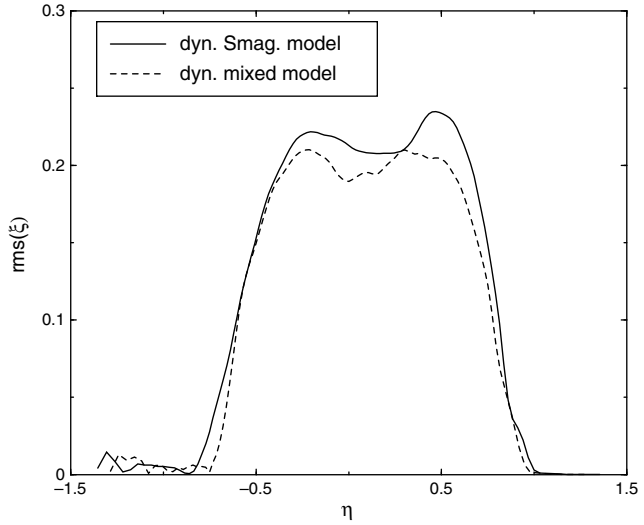

Fig. 12. Comparison of RMS passive scalar obtained with the two subgrid models – $M_c = 0.16$.

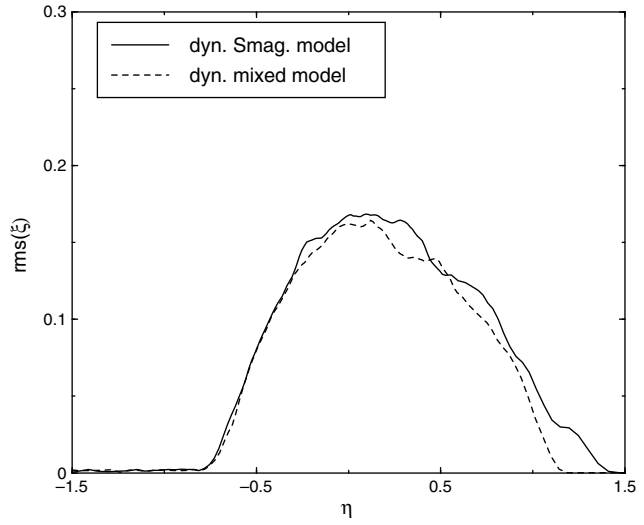

Fig. 13. Comparison of RMS passive scalar obtained with the two subgrid models – $M_c = 1.1$.

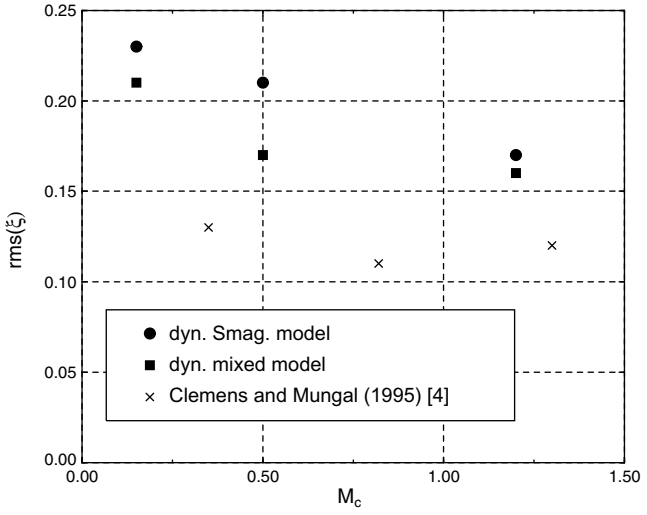

Fig. 14. Dependence of peak passive scalar RMS on M_c.

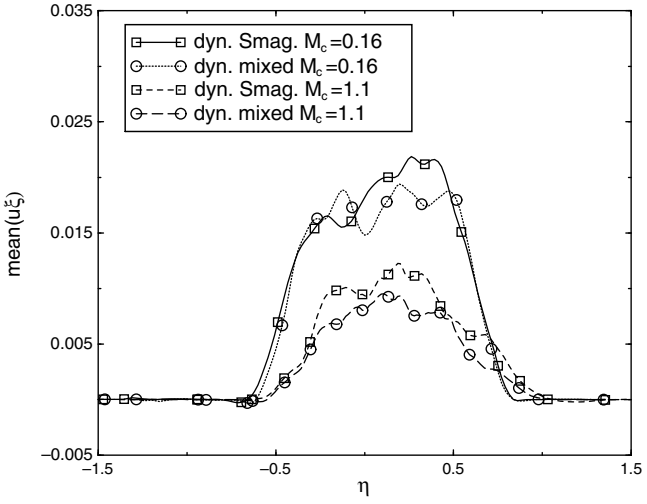

Fig. 15. Comparison of $\overline{u\xi}$ profiles obtained with the two subgrid models and for the two extreme M_c.

7. Evolution of the passive scalar probability density functions

The probability density function (PDF) of the mixture fraction obtained with the dynamic Smagorinsky model for $M_c = 0.16$ and for $M_c = 1.1$ in the self-similarity zone are shown in Figs. 17 and 18. The PDF are presented for five lateral locations, ranging from the mixing layer centerline outwards through the upper and lower shear regions. The filled symbols across the tops of the plots give the mean values associated with the PDF drawn with the corresponding unfilled symbols.

For the low convective Mach number mixing layer, the PDF are broad with low peaks that do not correspond exactly to the mean values. Except in the middle of the mixing layer, the most probable value jumps from $\xi = 0$ to $\xi = 1$ with increasing η. This corresponds to a non-marching comportment. In a non-marching PDF, the most probable value remains at a constant location across the layer irrespective to the local mean value. This type of PDF characterizes mixing which is dominated by large-scale engulfing of pure fluid from external streams. This non marching behavior is in agreement with the incompressible results of Konrad [25], Koochesfahani and Dimotakis [29], and of Masutani and Bowman [30]. But it does not agree with the results of Clemens and Mungal [4]. However, the difference in marching versus non-marching PDFs is also tied to how developed the turbulence is. This point is discussed in the article of Karasso and Mungal [31]. In the case of the plane jet [15] the PDFs also change from marching to no marching and tilted during the evolution of the scalar field. The differences with the results of Clemens and Mungal [4] might come from a much higher Reynolds number compared to our simulations.

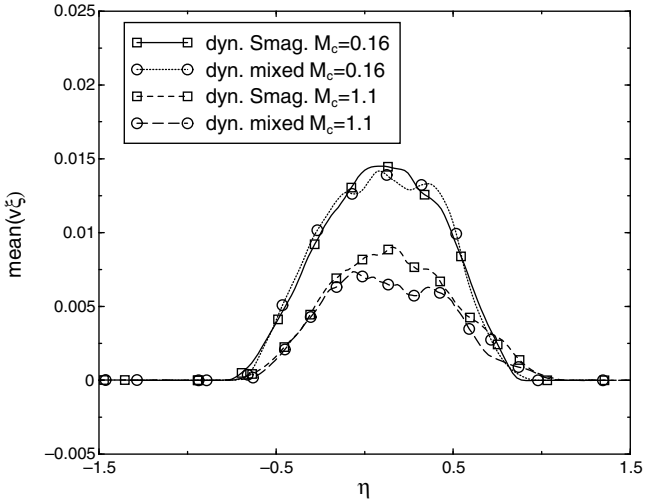

Fig. 16. Comparison of $\overline{v\xi}$ profiles obtained with the two subgrid models and for the two extreme M_c.

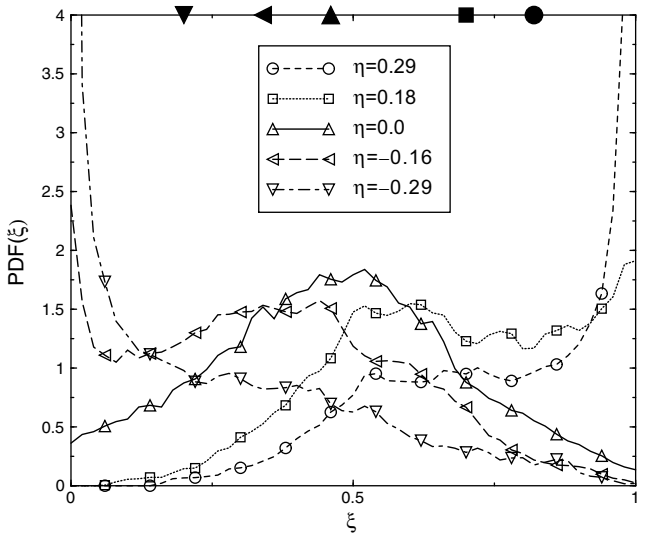

Fig. 17. PDF of the mixture fraction at various transverse locations – $M_c = 0.16$.

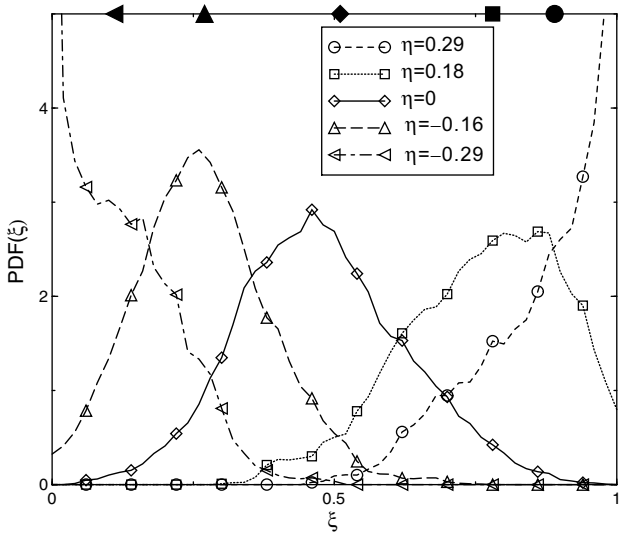

Fig. 18. PDF of the mixture fraction at various transverse locations – $M_c = 1.1$.

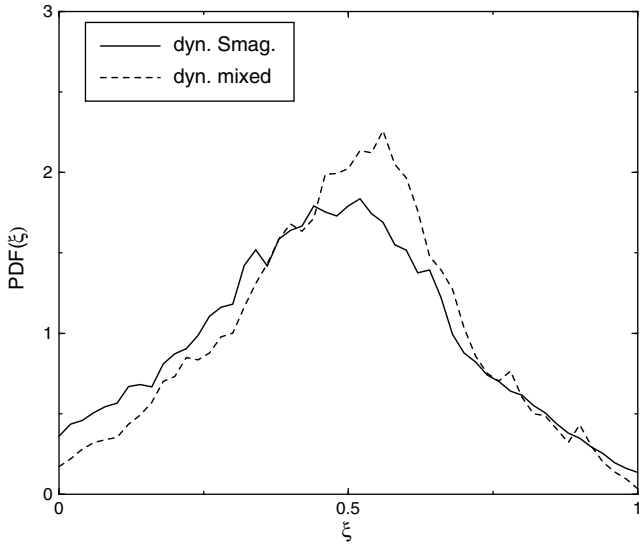

Fig. 19. PDF of the mixture fraction at $\eta = 0$ – $M_c = 0.16$.

For the supersonic mixing layer, the PDF peaks correspond to the mean value of the passive scalar. In a marching PDF, the most probable value varies across the layer following the local mean value of the scalar. This type of PDF is characteristic of the classical notion of mixing dominated by the small scales of motion. The peak scalar marches across the mixing layer, similar to the results of Clemens and Mungal [4] in compressible mixing layers. Compressibility acts to make the PDFs march, even at low Reynolds number. This result was also discussed in the numerical simulation of Freund et al. [11].

Figs. 19 and 20 show the PDF of the mixture fraction obtained with the two subgrid models for $M_c = 0.16$ and for $M_c = 1.1$ at the transverse location corresponding to the similarity coordinate $\eta = 0$. There is a weak trend of narrower and taller PDFs with increasing convective Mach number.

Broader PDFs indicate that a larger range of concentration levels are detected at a given location. These broad PDFs are also responsible for the larger RMS fluctuations found at the lower convective Mach number. Large eddies will broaden the PDFs since fluid can be transported from regions far from the measurement location. On the contrary, a layer that is dominated by small eddies will produce concentration PDFs that are more narrow. This argument suggests that scalar transport in compressible layer may occur through smaller-scale eddies. Those arguments were also developed in Clemens and Mungal [4].

8. Scalar field visualisation

The next Figs. 21 and 22 show the contours of the filtered instantaneous scalar obtained with the dynamic mixed model for the two convective Mach numbers

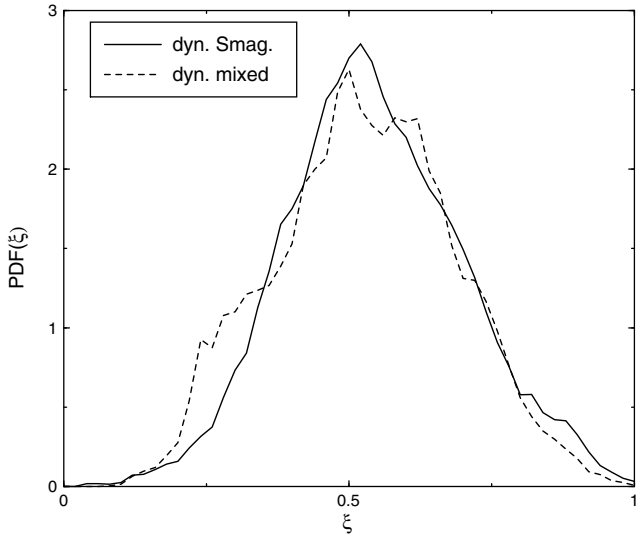

Fig. 20. PDF of the mixture fraction at $\eta = 0$ – $M_c = 1.1$.

$M_c = 0.16$ and $M_c = 1.1$. In the transition zone, the mixing layer thickness stays relatively constant. Then, the shear layer gets perturbed and rolls up into vortical structures. In this region, the thickness of the mixing layers increases linearly. For $M_c = 0.16$, the mixing layer thickness begins to increase after about 200 δ_{θ_0} and for $M_c = 1.1$ its begins to increase after about 500 δ_{θ_0}. The increase of the transition zone with the convective Mach number is confirmed by experimental results.

In the high Mach number mixing layer, the mixing layer is pushed down toward the subsonic side. This is consistent with the observation in the experiments where a similar downward motion due to transverse pressure non-equilibrium was observed.

At low M_c, the turbulent structures appear primarily as rollers. There are large intrusions of free-stream fluid into the layer. At high M_c, the structures are more irregular and appeared as jagged, irregular structures. When the convective Mach number increases, the low Mach number organized structures are lost and the size of the structures decreases [4].

A zoom of the contours are presented in the Figs. 23 and 25. The size of the two boxes are the same.

Zoom of the contours of the mixing index $\xi(1-\xi)$ are also presented on the Figs. 24 and 26. This quantity is equal to zero outside the shear layer so that the structures appear more clearly than in the case of the isocontours of the passive scalar. For the low Mach number mixing layer, the Figs. 23 and 24 reveals the domination of the layer by coherent structures. The structures are smaller for the high convective Mach number mixing layer (Figs. 25 and 26). They appear less elliptical and typically have a more disorganized appearance. The decrease in organization of the layer with increasing Mach number is in general agreement with the imaging results of Clemens and Mungal. The isovalues produced by the mixing index are very similar to isovalues of the passive scalar and the same conclusions can be made.

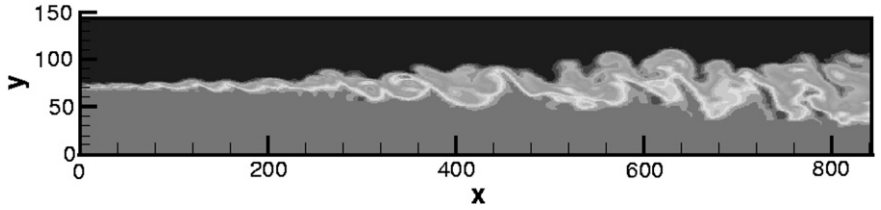

Fig. 21. Contours of the passive scalar in a $x - y$ plane. Dynamic mixed model – $M_c = 0.16$.

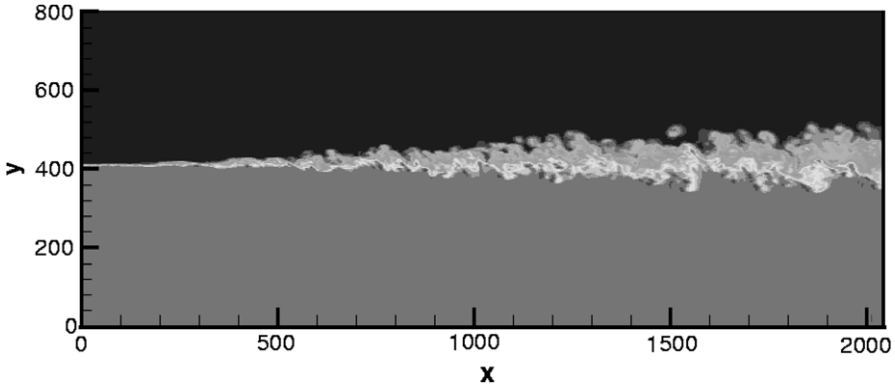

Fig. 22. Contours of the passive scalar in a $x - y$ plane. Dynamic mixed model – $M_c = 1.1$.

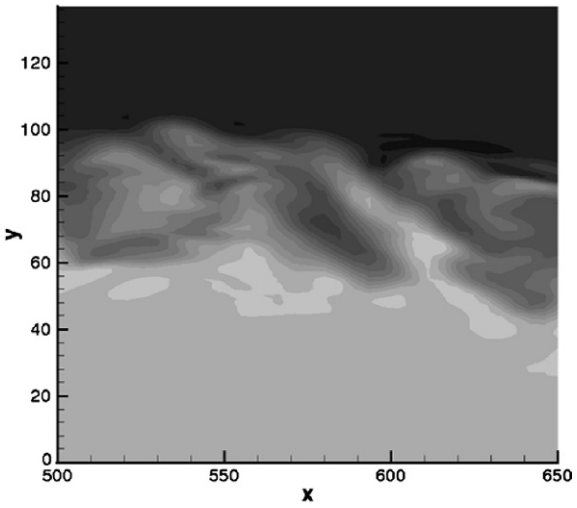

Fig. 23. Zoom of the contours of the passive scalar in the self-similarity region. Dynamic mixed model $M_c = 0.16$.

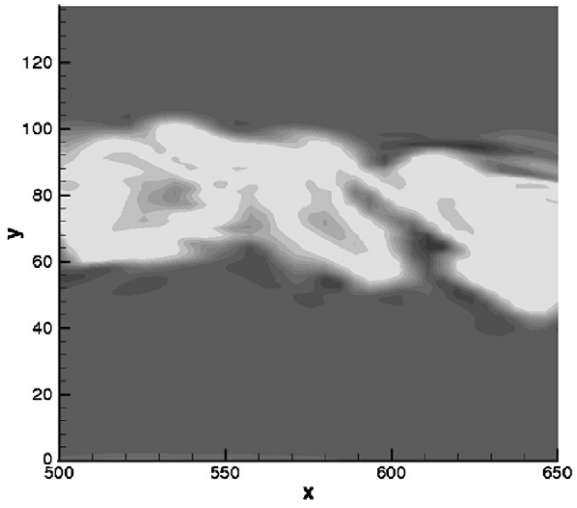

Fig. 24. Zoom of the contours of the mixing index in the self-similarity region. Dynamic mixed model $M_c = 0.16$.

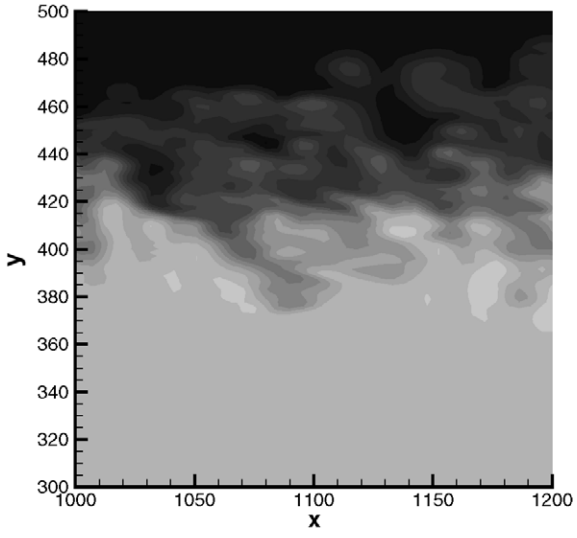

Fig. 25. Zoom of the contours of the passive scalar in the self-similarity region. Dynamic mixed model $M_c = 1.1$.

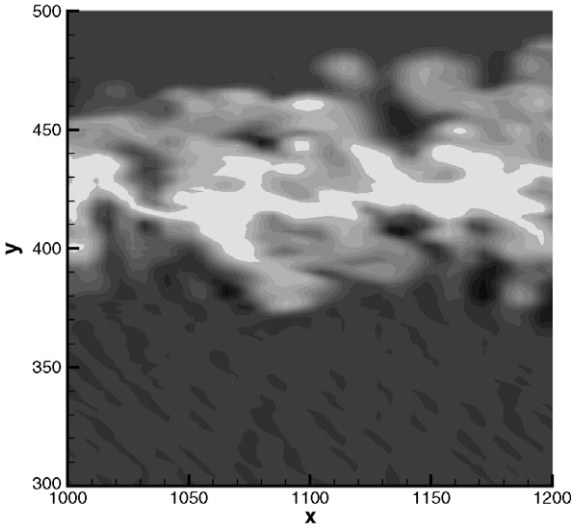

Fig. 26. Zoom of the contours of the mixing index in the self-similarity region. Dynamic mixed model $M_c = 1.1$.

9. Conclusion

LES of spatially developing mixing layers at three different convective Mach numbers are carried out. Two subgrid models are compared: the dynamic Smagorinsky model and the dynamic mixed model. The growth rate and the velocity statistics of the compressible mixing layer are suppressed relative to its incompressible counterpart. Quantitative comparisons of the mean and RMS of velocity fluctuations show that both models reasonably resolve the shear layer.

The results on the scalar properties (mean and RMS) confirm that the two models can accurately capture the physics of compressible mixing. Good quantitative agreement with experimental data is obtained. The principal compressibility effects such as the decrease of the RMS statistics, qualitative changes in the PDFs and in the structures shape are predicted by both models. However, from *a priori* tests, the dynamic mixed model is known to provide better representation of the subgrid stress tensor. *A posteriori* simulations, in the case of the plane jet also confirmed this fact by comparison with DNS results. The use of the dynamic mixed model is then recommended.

References

[1] D. Papamoschou, A. Roshko, The compressible turbulent shear layer: an experimental study, J. Fluid. Mech. 197 (1988) 453–477.
[2] G.S. Elliot, M. Samimy, Compressibility effects in free shear layers, Phys. Fluids A 2 (7) (1990) 1231–1240.
[3] S. Barre, C. Quine, J. Dussauge, Compressibility effects on the structure of supersonic mixing layers: experimental results, J. Fluid Mech. 259 (1994) 47–78.
[4] N.T. Clemens, M.G. Mungal, Large-scale structure and entrainment in the supersonic turbulent mixing layer, J. Fluid Mech. 284 (1995) 171–216.
[5] S.G. Goebel, J.C. Dutton, H. Krier, J.P. Renie, Mean and turbulent velocity measurements of supersonic mixing layers, Exp. Fluids 8 (1990) 263–272.

[6] S.G. Goebel, J.C. Dutton, Velocity measurements of compressible, turbulent mixing layers, AIAA J. 29 (4) (1991) 538–546.
[7] A. Kourta, R. Sauvage, Computation of supersonic mixing layers, Phys. Fluids 14 (11) (2002) 3790–3797.
[8] N.D. Sandham, W.C. Reynolds, Three-dimensional simulations of large eddies in the compressible mixing layer, J. Fluid Mech. 224 (1991) 133–158.
[9] N.T. Clemens, P.H. Paul, Scalar measurements in compressible axisymmetric mixing layers, Phys. Fluid 7 (5) (1994) 1071–1081.
[10] C. Pantano, S. Sarkar, A study of compressibility effects in the high-speed turbulent shear layer using direct simulation, J. Fluid Mech. 451 (2002) 329–371.
[11] J.B. Freund, P. Moin, S. Lele, Compressibility effects in a turbulent annular mixing layer. Part 2. Mixing of a passive scalar, J. Fluid Mech. 421 (2000) 269–292.
[12] V. Sankaran, S. Menon, LES of scalar mixing in supersonic mixing layers, Proc. Combust. Institute 30 (2005).
[13] C. Le Ribault, Large Eddy simulation of compressible mixing layers, International Journal of Dynamics of Fluid 1 (1) (2005) 86–111.
[14] C. Le Ribault, S. Sarkar, S.A. Stanley, Large Eddy simulation of a plane jet, Physics of Fluids 11 (10) (1999) 3069–3083.
[15] C. Le Ribault, S. Sarkar, S. Stanley, Large-Eddy simulation of evolution of a passive scalar in a plane jet, AIAA J. 39 (8) (2001) 1509–1516.
[16] Na. Yang, On the large Eddy simulation of scalar transport with Prandtl number up to 10 using dynamic mixed model, J. Mechan. Technol. 19 (3) (2005) 913–923.
[17] J. Smagorinsky, General circulation experiments with the primitive equations, Mon. Weather Revue 91 (1963) 99–164.
[18] M. Germano, U. Piomelli, P. Moin, W.H. Cabot, A dynamic subgrid-scale Eddy viscosity model, Phys. Fluids A 3 (7) (1991) 1760–1765.
[19] J. Bardina, J.H. Ferziger, and W.C. Reynolds, Improved turbulence models based on LES of homogeneous incompressible turbulent flows, Rep. TF-19, Department of Mechanical Engineering, Stanford, 1984.
[20] S.K. Lele, Compact finite difference schemes with spectral like resolution, J. Comp. Phys. 103 (1) (1992) 16–42.
[21] S.T. Zalesak, Fully multidimensional flux-corrected transport algorithms for fluids, J. Comput. Phys. 31 (3) (1979) 335–362.
[22] S.A. Stanley, S. Sarkar, J.P. Mellano, A study of flow-field evolution and mixing in a planar turbulent jet using direct numerical simulation, J. Fluid Mech. 450 (2002) 377–407.
[23] K.W. Thompson, Time dependent boundary conditions for hyperbolic systems, J. Comput. Phys. 68 (1) (1987) 1–24.
[24] F.Q. Hu, On absorbing boundary conditions for linearized Euler equations by a perfectly matched layer, J. Comput. Phys. 129 (1) (1996) 201–219.
[25] J.H. Konrad, An experimental investigation of mixing in two-dimensional turbulent shear flows with applications to diffusion-limited chemical reactions. PhD thesis, California Institute of Technology, 1977.
[26] H.E. Fiedler, Transport of heat across a plane turbulent mixing layer, Adv Geophys. 18 (1974) 93–109.
[27] R.G. Batt, Turbulent mixing in passive and chemically reacting species in a low-speed shear layer, J. Fluid Mech. 82 (1977) 53–95.
[28] T.C. Island, W.D. Urban, M.G. Mungal, Quantitative scalar measurements in compressible mixing layers, AIAA Paper 96-0685, 34th Aerospace Sciences Meeting, Reno NV, 1996.
[29] M.M. Koochesfahani, P.E. Dimotakis, Mixing and chemical reactings in a turbulent liquid mixing layer, J. Fluid. Mech. 170 (1986) 83–112.
[30] M. Masutani, C.T. Bowman, The structure of a chemically reacting plane mixing layer, J. Fluid Mech. 172 (1986) 93–126.
[31] P.S. Karasso, M.G. Mungal, Scalar mixing and reaction in plane liquid shear layers, J. Fluid Mech. 323 (1996) 23–63.